ISSN 1070-3632, Russian Journal of General Chemistry, 2012, Vol. 82, No. 12, pp. 2088–2099. © Pleiades Publishing, Ltd., 2012.
Original Russian Text © R.Sh. Abiev, I.V. Lavretsov, 2011, published in Rossiiskii Khimicheskii Zhurnal, 2011, Vol. 55, No. 2, pp. 60–70.

Hydrodynamics and Mass Exchange in Gas−Liquid Slug Flow in Microchannels

R. Sh. Abiev and I. V. Lavretsov

St. Petersburg State Technological Institute (Technical University), Moskovskii pr. 26, St. Petersburg, 190013 Russia
e-mail: rufat.abiev@gmail.com

Received May 5, 2011

Abstract—The present state of hydrodynamics and mass transfer studies in segmented gas−liquid flow in microchannels has been analyzed. It has been shown that such parameters as gas bubble velocity, gas hold-up, relative gas bubble length, pressure drop, mass transfer coefficients from gas bubbles to liquid slugs and to liquid film, as well as mass transfer coefficient from liquid to channel wall can be satisfactorily predicted. Nevertheless, some correlations were obtained under definite conditions and should be summarized. The purpose of further research is to develop reliable methods for calculation of mass transfer coefficients as functions of channel geometry, phase properties, and phase velocities in mini- and microchannels.

DOI: 10.1134/S1070363212120298

NOTATION

a – phase contact surface area, m^2/m^3
A_b – cross-sectional area of a bubble, m^2
A_c – cross-sectional area of a capillary, m^2
A_f – cross-sectional area of a film, m^2
C_1 – dimensionless constant
C_0 – dimensionless constant of the slipp model
d_c – capillary diameter, m
D – diffusion coefficient, $m^2\ s^{-1}$
g – gravity, $m\ s^{-1}$
J – dimensionless constant of the motion of the fastest-moving liquid elements relative to a bubble, reduced to the mean velocity of liquid slug
k – mass-transfer coefficient , $m\ s^{-1}$
L – capillary length, m
L_f – liquid film length, m
L_s – reduced length of liquid slug, m
L_{UC} – cell length, m
n – dimensionless coefficient
N_{UC} –number of cells along the capillary, rel. units
p – pressure, Pa
Δp_{trans} – pressure drop in a capillary, associated with change of liquid slug velocity profile, Pa
$\Delta p \Delta F$ – pressure drop associated with new surface formation on bubble motion, Pa
Q_f – liquid film mean volumetric flow rate, $m^3\ s^{-1}$
q_b –gas volumetric flow rate due to bubble motion (local), $m^3\ s^{-1}$
q_f –liquid film volumetric flow rate (local), $m^3\ s^{-1}$;
q_s –liquid slug volumetric flow rate (local), $m^3\ s^{-1}$
R – capillary radius, m
R_b – bubble radius, m
t_f – contact time of gas bubble with liquid film, s
u_l – local medium velocity, $m\ s^{-1}$
U_b – bubble velocity, $m\ s^{-1}$
U_f – liquid film velocity, $m\ s^{-1}$
U_G – gas velocity reduced to the total capillary cross-sectional area, $m\ s^{-1}$
U_L – liquid velocity reduced to the total capillary cross-sectional area, $m\ s^{-1}$
U_s – liquid slug velocity, reduced to the total capillary cross-sectional area (two-phase flow velocity), $m\ s^{-1}$
w – relative bubble velocity, $m\ s^{-1}$
w_b –slip velocity between bubbles and the stagnant liquid, $m\ s^{-1}$
x – axial coordinate, m
β – gas volumetric flow fraction, rel. units
γ – angle between the vector of two-phase flow velocity in a capillary U_s and the vector of gravity g
γ_m – roots of the second-order Bessel function: $J_2(\gamma) = 0$
δ –film thickness surrounding a bubble, m
ε_A – relative bubble surface area, rel. units
ε_L – relative bubble length, rel. units
ε_V – gas void fraction, rel. units
η – ratio of bubble velocity to two-phase flow velocity, $\eta = U_b/U_s$, rel. units
μ – dynamic viscosity, Pa s
ν – kinematic viscosity coefficient, $m^2\ s^{-1}$

ρ – dencity, kg m^{-3}
σ – interfacial tension, N m^{-1}

Similarity Criteria

$\mathrm{Bo} = \dfrac{(\rho_1 - \rho_2)d_c^2 g\cos\gamma}{\sigma}$ – modified Bond number;

$\mathrm{Ca} = \dfrac{\mu_1 U_b}{\sigma}$ – capillary number;

$\mathrm{Ca_s} = \dfrac{\mu_1 U_s}{\sigma}$ – capillary number calculated from U_s;

Ca* – critical capillary number;

$\mathrm{Fo} = \dfrac{Dt_f}{\delta^2}$ – Fourier criterion reduced to liquid film thickness;

$\mathrm{Gr} = \dfrac{L}{d_c}\dfrac{1}{\mathrm{ReSc}} = \dfrac{L}{d_c}\dfrac{1}{\mathrm{Pe}}$ – Gretz criterion;

$\mathrm{Pe} = \mathrm{ReSc} = \dfrac{U_s d_c}{D}$ – Peclet number;

$\mathrm{Re} = \dfrac{\rho_1 U_s d_c}{\mu_1}$ – Reynolds number;

$\mathrm{Sh} = \dfrac{kd_c}{D}$ – Sherwood number;

$\mathrm{Sc} = \dfrac{\nu_1}{D}$ – Schmidt number;

$\mathrm{We} = \dfrac{\rho_1 U_s^2 d_c}{\sigma}$ – Weber number.

Indices

1 – continuous medium (liquid)
2 – disperse medium (gas)
a – gas–liquid system used to obtain Eq. (17)
b – bubble
c – capillary
d – gas–liquid system different from that used to obtain Eq. (17)
f – film
fs – liquid–solid film
gl – gas–liquid
gf – gas–liquid film
gs – gas–solid
g, G – gas
ls – liquid–solid
s – liquid slug
tot – total

INTRODUCTION

In the last two decades there has been fast-growing interest in the application of mini- and micro-technique in chemical engineering. High-efficiency micro heat exchangers, micromixers, microreactors, microextractors, micropumps, and microvalves have been developed and produced in small series [1]. A typical cross-sectional area of channels wherein material flow (gas, liquid, gas–liquid) is moving varies from 10 μm to 1–3 mm.[1]

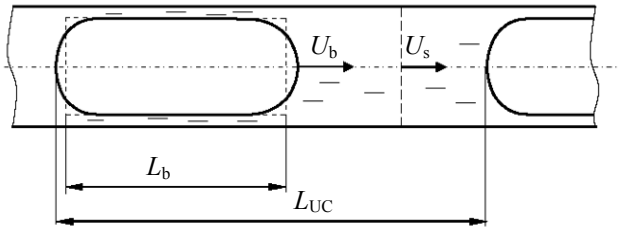

Fig. 1. Slug flow.

Microreactors can be competitive (i) in the case of fast reactions (from factions of a second to 3–5 min; in the latter case, helically-coiled pipes are used as reactors); (ii) when process rate is limited by mass transfer; and (iii) when fast removal of heat for reagents is required (for example, in the initial section of a continuous-flow reaction). The efficiency of processes in microreactors is explained by exceptionally high heat- and mass transfer coefficients in these devices (2 orders of magnitude higher than in traditional reactors) [1].

Microreactors are used to perform reactions in gas, gas–liquid, and liquid–liquid mixtures [2–4], as well as to synthesize ionic liquids [5]. One of the new trends in the development of microreactors is combining the benefits of microchannel flows and force fields, in particular, the microwave field [6, 7]. Applications of microreactors in fine organic synthesis, phase-transfer catalysis, hydrogen peroxide production, and other fields [8–10].

Microreactors can be divided into two types: single-channel and multichannel. Gas–liquid catalytic reactions are performed in one of the types of multichannel reactions, so-called monolithic catalysts (honeycomb catalysts) [8, 9] which represent a block of interconnected microchannels (hydraulic diameter from 0.3 to 1–3 mm) with catalyst-coated inside walls. Gas–liquid catalytic reactors are best performed under conditions of slug flow in microchannels [3, 8] (Fig. 1). In the slug flow of a gas–liquid mixture, gas bubbles

[1] Certain authors propose to distinguish the micro- and mini-scales. The commonly accepted boundary between them is set at about 100 μm. The upper boundary of the mini scale is, according to different authors, spans the range from 1 to 4–5 mm. No physically substantiated criterion for the boundary between the scales is still available.

are separated from each other by liquid slugs. This flow allows effective mixing inside the liquid slug due to so-called Taylor vortices, as well as shorter diffusion paths for gas molecules passing through the liquid film between bubbles and catalyst bed [3, 8, 9].

Mathematical simulation of the hydrodynamics and mass transfer in microreactors, which is the focus of the present paper, is a well-documented issue (for example, see [11–19]). In these works, partial differential equations were solved by the finite element or finite volume methods, i.e. each calculation involved a numerical experiment. Calculation results provided important information on streamlines, bubble shapes, and so forth, which is quite difficult to gain experimentally. At the same time, each solution of this kind is quite specific, and, therefore, the series of numerical experiments require further theoretical analysis and generalization.

Heat and mass transfer in microreactors are much dependent on the hydrodynamic parameters of the gas–liquid flow, and they are responsible for reaction yields and conver-sions [3, 18, 20]. In [21–24], an attempt was under-taken to develop a mathematical model which would allow to generalize numerous experimental results and results of mathematical simulation of the gas–liquid slug (Taylor) flow in microchannels (capillaries). This model was tested using published and own [25] experimental data.

Hydrodynamics of Gas–Liquid Slug Flow in Capillaries

Bubble and Liquid Velocities in Slugs and in Film

Bubble velocities in capillaries were determined, both theoretically and experimentally, in a numerous works [12, 15, 26–28], including basic research [29–31].

Abiev [21], based on the continuity equation and the momentum conservation equations for a heterogeneous liquid–gas (liquid–liquid) system under the assumption of axial flow symmetry and prevalence of interfacial tension and viscous friction forces over inertia forces (Weber number We << 1), developed a mathematical model of the hydrodynamics of gas–liquid slug flow in capillaries:

$$U_f A_f + U_b A_b = U_s A_c, \tag{1}$$

$$\frac{\delta}{R} = \frac{1.34\mathrm{Ca}^{2/3}}{1 + 3.33\mathrm{Ca}^{2/3}}, \tag{2}$$

$$q_f = \frac{\pi}{8\nu_1}\left(g_x - \frac{1}{\rho}\frac{\partial p}{\partial x}\right)(R^2 - R_b^2) - \pi C_1\left(\frac{R^2 - R_b^2}{2} - R_b^2 \ln\left[\frac{R}{R_b}\right]\right), \tag{3}$$

$$q_b = \frac{\pi}{4} g_x \left[\frac{R_b^2(R^2 - R_b^2)}{\nu_1} + \frac{R_b^2}{2\nu_2}\right] - \frac{\pi}{4}\frac{\partial p}{\partial x}\left[\frac{R_b^2(R^2 - R_b^2)}{\mu_1} + \frac{R_b^4}{2\mu_2}\right] - \pi C_1 R_b^2 \ln\left(\frac{R}{R_b}\right), \tag{4}$$

$$\partial p/\partial x = [(G_2 - G_3)g_x - q_s]/G_1. \tag{5}$$

where g_x is the projection of the gravity vector on the x axis:

$$G_1 = \frac{\pi}{8}\left[\frac{R^4 - R_b^4}{\mu_1} + \frac{R_b^4}{2\mu_2}\right],$$

$$G_2 = \frac{\pi}{8}\left[\frac{R^4 - R_b^4}{\nu_1} + \frac{R_b^4}{\nu_2}\right], \tag{6}$$

$$G_3 = \frac{\pi}{4}\frac{\rho_1 - \rho_2}{\mu_1} R_b^2(R^2 - R_b^2).$$

The model was closed by Eq. (2) (the Aussillou–Quéré equation [31]) for the film thickness surrounding a bubble δ. The model was used velocity profiles in a bubble, film, and liquid slug under the following boundary conditions: type 4 superficial gas velocity and zero velocity at capillary wall. The calculation results are well consistent with experimental data [15, 27].

In [21, 22], theoretical substantiation was given to the bifurcation dependence of the slip velocity between bubbles and a two-phase mixture for the upward and downward flows, which was previously observed in the experiment [27]. The reasons for bubble hold-up in narrow capillaries sealed on one end were explained [21]. It was shown that the tangential stress on the bubble (droplet) surface and the pressure gradient along a bubble can be fairly large ($\partial p/\partial x \approx 1000$ Pa m^{-1}), and this controls the interface shape [32]. Calculations by the developed model gave evidence for the asymptotic bubble velocity profile ($\eta = U_b/U_s \approx 2.5$), previously observed in the experiment [27].

Circular and Bypass Flow Regimes

The slug flow regimes can be arbitrarily divided into two types: circular and bypass (Fig. 2). In the first case, liquid slugs are discrete, since their intervening gas bubbles almost span the cross-sectional area of the capillary; the liquid film between the bubble and the capillary wall is 10–100 μm. The bypass flow regime takes place, when the liquid film between the bubble and the capillary wall occupies about 30% of the cross-sectional area, which results in a longitudinal liquid flow past a bubble.

The circular Taylor flows are among the principal factors of intensification of heat and mass transfer [16, 18]. Therefore, to calculate the hydrodynamics of the liquid flow in capillaries, a priori information on circulation in liquid slugs is necessary.

The mathematical model of the hydrodynamics of gas–liquid slug flow in capillaries, developed in [21], was used for theoretical substantiation of the boundary between the bypass and circulation flows past bubbles in gas–liquid slug flow [22]. The velocity profile in a liquid slug is parabolic, and the maximum liquid velocity in the slug is $\max(u_1) = 2U_s$. The velocity of the fastest-moving unit liquid volumes relative to a bubble, reduced to the mean velocity of the liquid slug, is given by the following equation:

$$J = \frac{\max(u_1) - U_b}{U_s} = \frac{2U_s - U_b}{U_s} = 2 - \frac{U_b}{U_s}. \quad (7)$$

In [22], a criterion J of the transition from a circular flow regime to a bypass flow regime was proposed: circular at $J > 0$ ($U_b/U_s < 2$) and bypass at $J < 0$ ($U_b/U_s > 2$). This criterion was tested on various liquids, specifically water, decane, and tetradecane [15], two silicon oils [27], as well as modified silicon oils with interfacial tensions σ of 0.2 and 0.004 N m^{-1}, respectively.

The generalized criterion of the balance of gravity and surface forces, used in [22], was a modified Bond number which accounts for the direction of gas–liquid flow in a capillary relative to capillary position:

$$\mathrm{Bo} = \frac{(\rho_1 - \rho_2) d_c^2 g \cos\gamma}{\sigma}. \quad (8)$$

The critical capillary number for the circular–bypass transition was approximated as follows [22]:

$$\mathrm{Ca}^* = 0.7378 + 0.0408\,\mathrm{Bo} + 3.5794\times10^{-4}\,\mathrm{Bo}^2 - 1.0799\times10^{-5}\,\mathrm{Bo}^3. \quad (9)$$

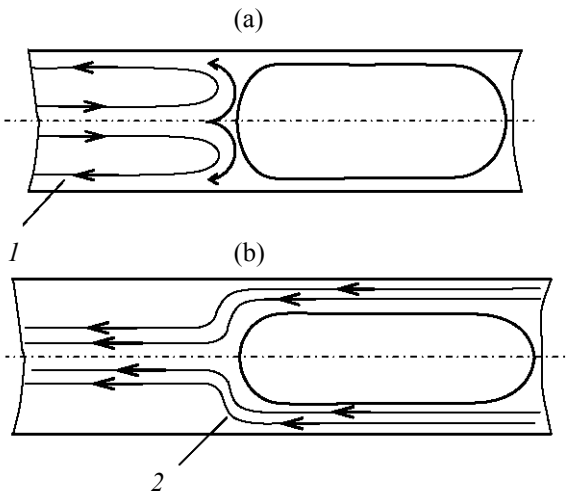

Fig. 2. Schematic representation of flow regimes: (a) circulation flow regime and (b) bypass flow regime. Liquid flow lines at the (*1*) circulation and (*2*) bypass flow regimes.

Contrary to what was proposed by Tsoligkas et al. [16], Abiev [33] could show, analytically and by numerical simulation, that circulation develops even in very short liquid slugs, at least in those having the capillary diameter-to-liquid slug length ratio $d_c/L_s \le 15$.

Gas Void Fraction and Relative Bubble Length

Bubble and slug lengths were shown to have an essential impact of the intensity of mass transfer in capillaries from gas to liquid and further to capillary wall [18, 20, 34, 35]. Therefore, in studying the hydrodynamics of flows in capillaries one should know the gas void fraction in a gas–liquid mixture and the relative length of bubbles.

In the works on the hydrodynamics of slug flow in capillaries, for example, in [36, 37], expressions relating the gas void fraction ε_V to the gas volumetric flow fraction β (the fraction of the gas volumetric flow in the total flow), or a simple equality $\varepsilon_V \approx \beta$, or Armand's correlation $\varepsilon_V \approx 0{,}833\ \beta$ [38]. Therewith, the bubble velocity U_b is related to the two-phase flow velocity as follows: $U_b = C_0 U_s + w_b$ [36, 37].

These approximations are acceptable at low velocities of low- and moderate-viscosity media, i.e. for the capillary numbers Ca << 1, when bubble velocities are only slightly higher than two-phase flow velocities [23].

Relationship of the gas void and gas volumetric flow fractions in a gas–liquid mixture in capillaries with diameters of 530 μm and smaller, was studied in [39, 40]. Quite specific flow regimes and an

anomalous dependence of gas void fraction on gas volumetric flow fraction were observed for 100- and 50-μm capillaries. In [23], this deviation was explained by an incorrect experiment design.

The following equation was obtained in [23] for the gas volumetric flow fraction

$$\beta = \frac{q_b\varepsilon_L}{q_s(1-\varepsilon_L) + q_f\varepsilon_L + q_b\varepsilon_L} . \quad (10)$$

As shown, the Armand formula is only acceptable at very low capillary numbers (Ca ≈ 10^{-4}–10^{-2}).

A relationship between gas void fraction and bubble parameters (relative surface area, relative length) was found for a gas–liquid flow in a capillary [23]:

$$\varepsilon_V = \varepsilon_A\varepsilon_L. \quad (11)$$

It was shown that the gas void fraction is dependent not only on the gas volumetric flow fraction, but also on the capillary number, Weber number, and flow direction [23].

Pressure Drop of the Slug Flow in Capillaries

Much research effort is being focused on the problem of pressure drop over capillary length in a gas–liquid mixture flowing through a capillary [15, 26, 28, 39–43], as well as local pressure drops due to expansion and compression of a gas–liquid flow [44]. Note that pressure drop predetermines the choice of auxiliary equipment for pushing the gas–liquid mixture through reactor. It relates to energy consumption and constitutes one of the key parameters of the equipment.

The pressure drop is considered to be most contributed by the frictional pressure drop of liquid slugs, determined by the Hagen–Poiseuille equation for a developed laminar flow [15, 26, 28, 43]. It was found that the pressure drop of a gas–liquid flow in capillaries is several times higher than in a single-phase liquid flow, at equal flow velocities. This effect is explained in terms of the different superficial curvatures of the bubble head and tail [15]. Fukano et al. [26] suggested that a considerable pressure drop is associated with a sudden liquid film expansion to form a liquid, but this hypothesis have not been confirmed in the experiment. Taking into account that the liquid velocity is 2 orders of magnitude lower than the bubble velocity [21], whereas the bubble and liquid slug velocities are of the same order of magnitude, i.e. liquid slugs move (albeit with a certain slip) together with bubbles, it can believed that the contribution of this kind of pressure drop is inconsiderable.

Liu et al. [28] even obtained negative pressure drops for low-velocity gas–liquid media. In our opinion, this is explained by erroneous measurements or by that the authors of [28] accounted for the hydrostatic pressure of a gas–liquid column in a capillary and neglected the hydrostatic pressure of liquid in the side tube attached to pressure gauge.

Warnier et al. [43] obtained a modification of the model of Kreutzer et al. [15], based on the Bretherton formula [30] for pressure drop over a bubble, corrected using the Aussillous–Quéré formula [31] for Ca >> 0. The modified model of Warnier et al. [43] was found to better fit experimental data than the model of Kreutzer et al. [15]. However, since the experimental testing was performed in a narrow range of capillary numbers (2.3×10^{-3} < Ca < 8.8×10^{-3}), it still does not allow generalization. Moreover, the authors of [43] do not exclude an increase of pressure drop with increasing bubble velocity, which explained by the fact that gas tends to expand as it approaches the open end of the capillary.

Kawahara and Chung [39] have reviewed the methods of simulation of the pressure drop of gas–liquid flows in capillaries. The simplest of them is a method based on the homogeneous medium (without phase slip) model for pressure drop. The formal method of Lockhart and Martinelli [45], developed by Chisholm and Laird [46, 47], is considered more advanced. The fact that calculated results poorly fit experimental data prompts researchers for searching for adequate values of the *C* constant in the Lockhart–Martinelli equation not only for each flow type, but also for different capillary dimensions.

Abiev [24] has analyzed the contributions of different kinds of the pressure drop of a gas–liquid medium in capillaries [24]. In addition to the previously developed model of the hydrodynamics of slug gas–liquid flow [21–23], a mathematic model to describe the pressure drop due to a change of the velocity profile in liquid slugs Δp_{trans} and due to the formation and renewal of the interfacial surface on bubble motion $\Delta p\Delta_F$:

$$\Delta p_{trans} = aN_{UC}L_s\left\{1 + \frac{1}{2bL_s}\left[1 - \exp(-bL_s)\right]\right\}, \quad (12)$$

where $a = 8\mu U_s/R^2$ and $b = \nu\gamma_m^2/U_sR^2$ are constants [24],

$$\Delta p_{\Delta F} = \frac{2R_b}{R^2}\frac{w}{U_s}\frac{L_s}{L_{US}}\sigma. \quad (13)$$

It was shown that the tangential stresses on the bubble surface contribute much into the total pressure drop [24]. The bubble length has no effect of pressure drop, if the bubbles move with equal velocities, since the strongest pressure drop takes place on the bubble head surface [24]. The simulation results are fairly consistent with the experiment [16], and, therewith, $\Delta p_{trans} << \Delta p_{\Delta F}$. A better fit was obtained in [25].

Phase Distribution in Monolith Channels and Stability of the Gas−Liquid Flow in Microchannels

Many advantages of microreactors (more efficient catalyst use, lack of stagnant zones and overheat spots) stem, to a great extent, from two factors: (1) a uniform distribution of the continuous and disperse phases over the cross-sectional area of a multichannel apparatus and (2) a uniform distribution of the continuous and disperse phases along the channels. Obviously, the second factor in much dependent of the first one, provided the channels are absolutely identical with each other. Therefore, the information concerning phase distribution over channels (for multichannel systems) and over channel length is quite important for microreactor scale-up.

Unfortunately, until now little attention has been paid to the problem of phase distribution of the gas−liquid flow in capillaries, notwithstanding the fact that this problem may take on great significance in passing from single-channel lab-scale devices to multichannel commercial systems. In particular, a nonuniform phase distribution may entail a considerable difference in phase velocities in channels, a large dispersion of gas void fractions over channels, and, consequently, a large dispersion in flow velocities in neighboring channels.

The problem of the hydrodynamic stability of a gas−liquid mixture in honeycomb monolith reactors was first raised by Grolman et al. [48], who noted that a guaranteed supply of liquid and gas into all channels is effected by means of a dispenser like a shower nozzle or by means of a bubbled layer over monolith (at gas void fractions below 0.5). In that work, a downward gas−liquid flow was experimentally studied. It was theoretically shown that flow instability arises, when the gravity force and the flow friction force caused by the retarding effect of channel walls act in the same direction; inertia forces were neglected.

Reinecke and Mewes [49] considered a model of oscillations of the gas−liquid flow in a channel, which includes inertia forces, a buffer volume (hydroaccumulator) which fulfills the damping function, as well as damping properties of the gas−liquid mixture; the friction losses were calculated for a pure bubble-free liquid. Liang and Ma [50], too, neglected the pressure drop over gas bubbles but included compressibility of the gas−liquid mixture. Van Steijn et al. [51] described the velocity fluctuations of a gas−liquid mixture in a microchannel, associated with pressure pulsations on bubble formation both at the inlet and at the outlet of the microchannel.

On the Problems Associated with Elucidation of the Mechanism of Bubble Formation in Gas –Liquid Flow in a Channel and with Bubble Size Measurement

Gas –liquid mixtures are obtained using a great variety of instruments: from the simplest T- or Y-shaped mixers for single-channel devices [52] to alternating monolith sections tilted to each other at an angle of 45º and nozzles like a shower head [48], and also individual gas injection into each channel of multichannel systems is practiced. In view of the great diversity of techniques for preparing gas−liquid mixtures, no common regularities have yet been established in the formation of gas bubbles in such mixtures, and, therefore, no common approaches to bubble size measurements could be developed.

One of the first works on the mechanism of the entrance of a bubble into a capillary tube was performed by de Tezanos Pinto et al. 1997 [53]. Van Steijn et al. [54] made use of microscopic particle image velocimetry (micro-PIV) to find out that the bubble formed in a T-shaped mixer with a square cross section blocks the channel completely. It was shown that up to 25% of liquid moves slowly along channel angles together with the formed bubble.

Maps of Gas−Liquid Flow Regimes in Capillaries

Designers of commercial microreactors for liquid−gas or liquid−liquid systems should have a clear information about conditions for realization of one or another flow regime of the reaction mixture. To this end, flow regime maps are constructed, which represent a coordinate grid with the abscissa being generally the reduced gas velocity and the ordinate, the reduced liquid velocity. Even though the properties of liquids and the shapes of channel cross-sections varies from research to research, the regime boundaries

obtained by different authors [26, 36, 55, 56] generally quite satisfactorily coincide with each other. Bauer [57] constructed flow maps for the α-methylstyrene–nitrogen system in a channel with a square cross-section channel with a 1-mm hydraulic radius at pressures of 1, 20, and 40 bar. Even though the regime boundaries shifted with increasing pressure, their mutual positions remained unchanged. In the same work, the influence of liquid properties on flow regime boundaries at different pressures was also studied.

Certain researchers tried to construct universal flow regime maps, using different hydrodynamic criteria or their combinations. Suo and Griffith [58] studied the transition from the slug to bubbly flow in horizontal cylindrical tubes 0.5–0.7 mm in diameter, and proposed a product of the Reyinolds and Weber numbers as the transition criterion:

$$\mathrm{Re}\cdot\mathrm{We} = \frac{U_\mathrm{b} D \rho_l}{2\mu_l} \frac{U_\mathrm{b}^2 D \rho_l}{2\sigma} = 2.8\times10^5, \qquad (14)$$

where 2.8×10^{-5} is a "critical" product of ρ_l and μ_l for any liquid.

Evidence for this criterion was obtained in later works [36, 59]. However, Triplett et al. [59] mentioned that this formula does not fit experimental data for square-shaped horizontal capillaries.

Attempts to include gas and liquid parameters in flow mapping were undertaken. Suo and Griffith [58] studied a liquid–gas system (liquid: water, hexane, and octane; gas: helium, nitrogen, and argon). With all the liquid–gas combination studied, the simplexes ρ_g/ρ_l and μ_g/μ_l and the properties of gases were found to only slightly affect flow regimes and transition boundaries.

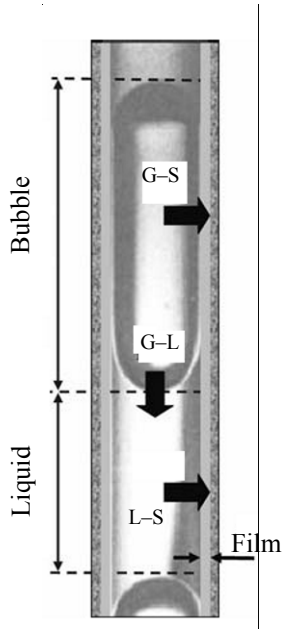

Fig. 3. Schematic representation of mass exchange flows at a slug flow regime [1].

The methods of determination of the flow regimes of gas–liquid media on the basis of the gas fraction have not yet been sufficiently developed [60]. Flow mapping using Re and Ca criterial numbers was proposed, which would allow such flow maps to be extended to different liquid–gas systems and channels of different geometries.

To conclude, we would like to note that extensive research has not yet led to the development of a complete model for precise prediction of flow regimes in capillaries.

Mass Transfer in a Gas–Liquid–Solid System under Taylor Flow

There are two possible ways of gas–liquid mass transfer in a single channel having an active component deposited on its inner walls, each including two stages: (1) transfer from the cylindrical surface of a bubble to the thin film of a liquid and further from the latter to the surface of a solid wall; (2) transfer from the head and tail of a bubble into a liquid slug and further to the surface of a solid wall (Fig. 3).

Below we present a brief review of the research on mass transfer in capillaries.

Assuming the mechanism of parallel mass transfer by each of the ways and mutual independence of the stage, Onea et al. [18] proposed the following expression for the total volumetric mass transfer coefficient:

$$k_\mathrm{tot}a_\mathrm{tot} = \left(\frac{1}{k_\mathrm{gf}a_\mathrm{gf}} + \frac{1}{k_\mathrm{fs}a_\mathrm{fs}}\right)^{-1} + \left(\frac{1}{k_\mathrm{gl}a_\mathrm{gl}} + \frac{1}{k_\mathrm{ls}a_\mathrm{ls}}\right)^{-1}. \qquad (15)$$

The problem of mass-transfer in the systems in question is solved in three ways: analytical solution of differential mass transfer equation; empirical methods based on the similarity theory; and numerical solution of differential mass-transfer equation.

In one of the first works on mass transfer, Jayawardena et al. [62] studied the process of solution of benzoic acid deposited on the walls of capillaries 2.350 and 3.094 mm in diameter, in a downward gas–liquid flow (water–air) with a velocity of 0.079–0.13 m s^{-1} under normal conditions. Horvath et al. [63] immobilized an enzyme on the inner wall of a capillary and performed hydrolysis catalyzed by this enzyme.

The following expression was obtained from the experimental data in [62, 63]:

$$\mathrm{Sh} = 3.51 \left(\frac{d_c}{L}\mathrm{Pe}\right)^{0.44} \left(\frac{L_s}{d_c}\right)^{0.44}. \quad (16)$$

The concentration of benzoic acid was measured at the capillary exit under the conditions of a single-phase liquid flow and a slug gas–liquid flow [62]. The concentration of benzoic acid in the latter case was found to be 2–3 times higher, implying intensified mass transfer under this flow regime.

Bercic and Pintar [20] studied separately the two stages of mass transfer (gas–liquid and liquid–solid) under normal conditions in an upward gas–liquid flow in capillaries with inner diameters of 1.5, 2.5, and 3.1 mm. Gas absorption in liquid was investigated on an example of methane solution in water. To study mass transfer from a liquid phase to a solid body (for example, the surface of a catalyst deposited on the inner walls of a capillary), experiments on solution of benzoic acid deposited on the walls of a capillary where a liquid is flowing. The influence of unit cell length L_{UC} (the unit cell is a gas bubble with its following liquid slug, Fig. 1), mean phase velocity, and gas void fraction on mass transfer coefficient was studied. The corresponding dependences were fitted by the following equations:

$$k_{gl}a_{gl} + k_{gf}a_{gf} = \frac{0.111U_s^{1.19}}{[(1-\varepsilon_V)L_{UC}]^{0.57}}, \quad (17)$$

$$k_{ls}a_{ls} + k_{fs}a_{fs} = \frac{0.069U_s^{0.63}}{[(1-\varepsilon_V)L_{UC} - 0.105L_{UC}\varepsilon_V]^{0.44}}. \quad (18)$$

The mass transfer coefficients calculated by Eqs. (16) and (18) much differ from each other. This result can be explained by the fact that Eqs. (17) and (18) do not include the capillary diameter, and the empirical coefficients are dimensionless. Kreutzer et al. [64] tried to overcome the latter drawback (dimensionless coefficients) by including the ratio of diffusion coefficients in Eq. (17):

$$(k_{gl}a_{gl} + k_{gf}a_{gf})_a = (k_{gl}a_{gl} + k_{gf}a_{gf})_b \left(\frac{D_a}{D_b}\right)^n. \quad (19)$$

The results of the experiments on oxygen absorption in water in a honeycomb catalytic reactor [65] were well fitted by Eq. (19).

Kreutzer et al. [64] also studied the hydrogenation of α-methylstyrene at a temperature of 323–413 K and a pressure of 10 bar in the channels of a honeycomb-structured support with a bed of an active component deposited on inner walls. Assuming that, at a mean flow rate of 0.2–0.8 m s^{-1}, the liquid film separating the gas bubble from the capillary wall is as thick as a diffusion layer, Eq. (15) was written in the following form:

$$k_{tot}a_{tot} = k_{gs}a_{gs} + \left(\frac{1}{k_{gl}a_{gl}} + \frac{1}{k_{ls}a_{ls}}\right)^{-1}, \quad (20)$$

$$k_{gs}a_{gs} = \frac{D}{\delta}. \quad (21)$$

The gas bubble–liquid slug mass transfer coefficient was calculated by Eq. (19), and for the case of transfer of dissolved gas from liquid to a solid surface (capillary wall), a formula obtained by computer simulation of heat transfer by analogy with mass transfer was proposed:

$$\mathrm{Sh} = 20(1 + 0.003\mathrm{Gr}^{-0.7}). \quad (22)$$

Comparison of the experimental total mass transfer coefficients with calculation showed that the proposed calculation procedure is not suitable enough for the described process. This can be explained by the ignoring of component diffusion inside the catalyst to active centers. In his later work, Kreutzer et al. [3] corrected Eq. (22):

$$\mathrm{Sh} = \sqrt{\alpha^2 + \frac{\beta}{\mathrm{Gr}}}, \quad (23)$$

$$\alpha = 40\left[1 + 0.28\left(\frac{L_s}{d_c}\right)^{-4/3}\right],$$

$$\beta = 90 + 104\left(\frac{L_s}{d_c}\right)^{-4/3}. \quad (24)$$

In simulating the process, the authors again turned to an analogy with the heat-transfer process and considered a simplified geometry of slug flow, namely liquid slugs were assumed to have a cylinder shape.

Gruber and Melin [66] performed an experimental study of liquid–solid mass transfer on an example of solution of a horizontally located copper capillary in a solution of sulfuric acid and potassium dichromate under normal conditions. The experimental results were compared with the results of computer simulation. Unlike the Kreutzer model [64], the task to be solved here was the task of solution (rather than heat transfer) of a substance at the liquid velocity

profile calculated by the Navier–Stokes equation. The authors of [66] highlighted three parameters controlling the rate of mass transfer: Peclet number Pe, relative length of luquid slug, and relative length of capillary:

$$\mathrm{Sh} = a_1 \tanh\left(a_2 \mathrm{Pe}^{a_3} + a_4\right) \times \tanh\left[a_5 \left(\frac{L_\mathrm{s}}{d_\mathrm{c}}\right)^{-a_6} + a_7\right] \times\left[1 - \left\{a_8 \mathrm{Pe} - a_9 \left(\frac{L_\mathrm{s}}{d_\mathrm{c}}\right)^{a_{10}} - a_{11}\right\} e^{-a_{12}\frac{L_\mathrm{s}}{d_\mathrm{c}}}\right]. \quad (25)$$

Here a_i are least-squares coefficients.

The dependence was obtained for the following conditions: Pe = 1600–400000, $L_\mathrm{S}/d_\mathrm{c}$ = 1–600, and L/d_c = 30–1000. The first and second terms of Eq. (25) includes the Peclet number and the relative length of liquid slugs, whereas the third term includes inlet effects and, to a lesser extent, the relative length of the capillary.

Comparison of the efficiency of mass transfer processes in continuous and slug flow regimes showed that in the latter case the mass transfer is 2–3 times more intensive and depends on the Peclet number and the relative length of the gas bubble. At small lengths of liquid slugs, the mass transfer is stronger intensified at Pe = 4000, than at Pe = 40000. In the case of long liquid slugs, the Peclet number is not so important.

Mass transfer under slug flow was also studied in [14, 67]. Van Baten and Krishna [67] considered the gas bubble–liquid mass transfer in an upward flow under normal conditions in capillaries with inner diameters of 1.5, 2, and 3 mm. By comparing the results of simulation and those obtained by the theoretical model developed by the authors, assessment of the influence of bubble velocity, unit cell length, film thickness and lengh, as well as diffusion coefficient on mass-transfer coefficient was performed.

Here, unlike the Kreutzer model [64], the bubbles were assumed to have the shape of cylinders with two hemispheres on the ends. The mass transfer from the hemispherical parts of the bubble was described in terms of the penetration model proposed by Higbi [68]:

$$k_\mathrm{gl} = 2\frac{\sqrt{2}}{\pi}\sqrt{2\frac{DU_\mathrm{b}}{d_\mathrm{c}}}. \quad (26)$$

The mass transfer from the cylindrical part of the bubble to the liquid film moving in a countercurrent to the flow under a laminar flow regime was described in terms of the model proposed by Pigford [68]:

$$k_\mathrm{gf} = \frac{Q_\mathrm{f}}{\pi d_\mathrm{c} L_\mathrm{f}} \ln\left(\frac{1}{\Delta}\right), \quad (27)$$

$$\Delta = 0.7857e^{-5.121\mathrm{Fo}} + 0.1001e^{-3921\mathrm{Fo}} + 0.0360e^{-105.6\mathrm{Fo}} + 0.0181e^{-204.7\mathrm{Fo}} + 1/4. \quad (28)$$

Equation (27) can also be written in the following form (by the results of processing of experimental data):

$$k_\mathrm{gf} = 2\sqrt{2\frac{D}{\pi t_\mathrm{f}}}\frac{\ln(1/\Delta)}{(1-\Delta)}, \ \mathrm{Fo} < 0.1, \quad (29)$$

$$k_\mathrm{gf} = 3.41\frac{D}{\delta}, \ \mathrm{Fo} > 1. \quad (30)$$

Equation (29) is valid for the case of a short phase contact, and Eq. (30) should be applied in all other cases, when liquid film is saturated with gas during a long phase contact.

In [68], the simulation was performed under the assumption of a stagnant gas–liquid flow and of the capillary wall moving at the bubble velocity, and, as always, it involved two steps: First, calculation of the velocity profile inside liquid slug and, second, solution of the task of mass transfer of gas from bubble surface to liquid.

The resulting data showed that at the same bubble velocity, the mass transfer coefficient increases with increasing length of liquid film and is unaffected by its thickness. Increasing bubble velocity enhances mass transfer both to film and to liquid slug, on account of shortening phase contact time. Comparison with the data in [20] revealed an essential disagreement with Eq. (17) at high bubble velocities and short liquid slugs and gas bubbles. Note that the experiments were performed at bubble velocities varied in the range 0.2–0.8 m s^{-1}, i.e. in the same range as Kreutzer et al. [64], who showed that Eq. (21) is a particular case of their theory.

Van Baten and Krishna [14] considered liquid–wall mass transfer (simulation conditions and procedure were similar to those in [68]). The following equations were proposed:

$$\mathrm{Sh} = \frac{\beta}{\mathrm{Gz}_\mathrm{t}^{\alpha}}, \quad (31)$$

$$\alpha = 0.61\mathrm{Gz}_\mathrm{s}^{0.025}, \quad (32)$$

$$\beta = \frac{0.5}{(Gz_s/\varepsilon_V)^{0.15}}, \quad (33)$$

$$Gz_s = \frac{L_s D}{d_c^2 U_b}, \quad (34)$$

$$Gz_t = \frac{(1-\varepsilon_V)LD}{d_c^2 U_b}. \quad (35)$$

The dependence of the Scherwood number on the Gretz criterion for a capillary is insensitive to bubble velocity and gas void fraction. The coefficient of mass transfer from liquid film to capillary wall is lower than that for mass transfer from liquid slug to wall, since at a high gas void fraction the bubble is longer, and, therefore, the bubble–film contact time is long enough to saturate the film. In the case of short liquid slugs, the contributions of the two processes compare with each other.

The simulation results allow a conclusion that the mass transfer is mostly contributed by three factors: gas void fraction, liquid slug length, and diffusion coefficient. Equations (31)–(35) were found to poorly fit the experimental data in [20] and [63].

Vandu et al. [69], in their study on oxygen absorption in water at flow velocities of 0.02–0.24 m s^{-1} in a honeycomb catalytic reactor that the transfer of dissolved gas from liquid slug to wall, established that for understanding mass transfer in the Taylor flow regime, it is necessity to account for the transfer of dissolved gas from liquid slag to wall. As judged from the plots presented in [69], Eqs. (26)–(30) and (36) rather poorly predict experimental data.

The mass transfer from gas bubble to liquid on an example of oxygen absorption in water was also studied in [70]. The obtained experimental data were compared with the results of calculations by Eqs. (26)–(30). The experiments were performed using round (inner diameters 1, 2, and 3 mm) and square cross-section capillaries (hydraulic diameter of the cross section 1 and 3 mm) in an upward gas–air flow.

In view of the data in [67], the authors concluded that the mass transfer is most contributed by gas transfer from the cylindrical part of the bubble to the liquid film. A simplified formula of mass transfer coefficient for engineering calculations was proposed:

$$k_{gf} + k_{gl} = 4.5\sqrt{\frac{DU_G}{L_{UC}}}\,\frac{1}{d_c}. \quad (36)$$

The formula is valid under the condition if

$$\sqrt{\frac{U_G + U_L}{L_s}} > 3.$$

takes values less than 3, a saturated liquid film is suggested. The maximum deviation of experimental data from the calculation by Eq. (36) is 30%, and the average deviation is 20%. Equation (17), too, poorly fitted the experimental data. The authors suggested that the reason for such deviations is in the conditions in which Eq. (17) was obtained in [20], namely, unit cell lengths of 220 mm and flow velocities of up to 0.16 m s^{-1}. Under such conditions, the film is rapidly saturated with gas. In [70], the cell length was 0.005–0.6 m and the flow rate was up to 0.09–0.65 m s^{-1}.

Tsoligkas et al. [71] studied the mass-transfer issues in the hydrogenation of but-2-yne-1,4-diol in a downward gas–liquid flow in a single ceramic capillary (inner diameter 1.69 mm) with catalyst-coated walls. The influence of liquid slug and bubble lengths on the reaction rate was estimated under varied gas and liquid velocities. The highest reaction rate was reached at L_s/d_c = 1.2, whereas the bubble length had no essential rate effect. By varying the length of liquid slug, the authors succeeded in increasing the process selectivity from 20 to 80%. These results showed that here the gas transfer through film to capillary wall is of secondary importance compared to the gas transfer to capillary wall through liquid slug. The mass transfer coefficient was calculated using Eqs. (19)–(21), as well as Eq. (18) modified by analogy with Eqs. (17) and (19). The calculated results well fitted the experimental data in the case when mass transfer was limited by the gas phase. If the process was limited by the concentration of but-2-yne-1,4-diol in the liquid phase, the calculation failed to fit the experiment.

In the considered works, the numerical solutions of the equations of mass transfer in the slug flow regime were based on the assumption of an axially symmetric flow, i.e. they related exclusively to round capillaries. Furthermore, the phase interface was preset, and the continuous medium was assumed to be the only mobile medium. These assumptions were overcome by Onea et al. [18], who made use of the finite volume method. In that work, 3D simulation of the mass-transfer process in an upward flow in single channels with square and triangle cross-sections and hydraulic diameters of 2 mm.

It should be noted that the liquid film separating the bubble from the capillary wall was always saturated.

The simulation results showed that short liquid slugs are preferred, when high gas concentrations in the liquid phase are necessary to be obtained over a short time, whereas long liquid slugs are preferred, when a large volume of gas is necessary to transfer into liquid. These data are generally consistent with the results in [14, 67]; however, true enough, in those works the film was initially not saturated. It was found that the mass transfer in triangle channels is more efficient than in rectangular channels, because in the former case a gas bubble assumes an ellipsoidal cross section, which favors a larger phase contact surface. Unfortunately, having performed a fairly deep analysis of the problem, the researchers proposed no equation for engineering calculations.

As seen from the present review, no general theory of mass transfer, which would account for the features of chemical reactions and diffusion inside a multichannel catalyst, has yet been developed. There are scarce experimental data for single channels and multichannel systems: All reported experiments were performed under normal conditions and in round capillaries.

CONCLUSIONS

Wide use of mini- and microdevices in industry is prevented, along with the limited number of studied reactions, by the insufficient understanding of the hydrodynamics and mass exchange in mini- and microchannels. Further research should focus on the development of reliable methods for calculation of mass-transfer coefficients as functions of the geometry of mini- and microchannels, properties of media, and phase velocities.

REFERENCES

1. Hessel, V., Löwe, H., Müller, A., and Kolb, G., *Chemical Micro Process Engineering. Processing and Plants*, Weinheim: Wiley–VCH, 2005, p. 288.
2. Hessel, V., Angeli, P., Gavriilidis, A., and Löwe, H., *Ind. Eng. Chem. Res*., 2005, vol. 44, no. 25, pp. 9750−9769.
3. Kreutzer, M.T., Kapteijn, F., Moulijn, J.A., and Heiszwolf, J.J., *Chem. Eng. Sci*., 2005, vol. 60, no. 22, pp. 5895−5916.
4. Borovinskaya, E.S. and Reshetilovskii, V.P., *Khim. Prom-st'*, 2008, vol. 85, no. 5, pp. 217−247.
5. Renken, A., Hessel, V., Lob, P., et al., *Chem. Eng. Proc*., 2007, vol. 46, no. 9, pp. 840−845.
6. Gao, P., Rebrov, E.V., Schouten, J.C., et al., *MRS Fall Meeting*, Boston, 2009.
7. He, P., Haswell, S.J., and Fletcher, P.D.I., *Lab Chip*., 2004, vol. 4, no. 1, pp. 38−41.
8. Bauer, T., Shubert, M., Lange, R., and Abiev, R.Sh., *Zh. Prikl. Khim*., 2006, vol. 79, no. 7, pp. 1047−1056.
9. Roy, S., Bauer, T., Al-Dahhan, M., Lehner, P., and Turek, T., *AIChE J*., 2004, vol. 50, no. 11, pp. 2918−2938.
10. Rebrov, E.V., *Khim. Tekhnol*., 2009, vol. 10, no. 10, pp. 595−604.
11. Edvinsson, R. K. and Irandoust, S., *AIChE J*., 1996, vol. 42, no. 7, pp. 1815−1823.
12. Taha, T. and Cui, Z.F., *Chem. Eng. Sci*., 2004, vol. 59, no. 6, pp. 1181−1190.
13. Taha, T. and Cui, Z.F., *Ibid*., 2006, vol. 61, no. 2, pp. 676−687.
14. Van Baten, J.M. and Krishna, R., *Ibid*., 2005, vol. 60, no. 4, pp. 1117−1126.
15. Kreutzer, M.T., Kapteijn, F., Moulijn, J.A., Kleijn, C.R., and Heiszwolf, J.J., *AIChE J*., 2005, vol. 51, no. 9, pp. 2428−2440.
16. Tsoligkas, A.N., Simmons, M.J.H., and Wood, J., *Chem. Eng. Sci*., 2007, vol. 62, no. 16, pp. 4365−4378.
17. Wörner, M., Ghidersa, B., and Onea, A., *Int. J. Heat Fluid Flow*, 2007, vol. 28, no. 1, pp. 83−94.
18. Onea, A., Wörner, M., and Cacuci, D.G., *Chem. Eng. Sci*., 2009, vol. 64, no. 7, pp. 1416−1435.
19. Wörner, M., *7th Int. Conf. on Multiphase Flow*, Tampa, 2010.
20. Bercic, G. and Pintar, A., *Chem. Eng. Sci*., 1997, vol. 52, nos. 21–22, pp. 3709−3719.
21. Abiev, R.Sh., *Teor. Osnovy Khim. Tekhnol*., 2008, vol. 42, no. 2, pp. 115−127.
22. Abiev, R.Sh., *Ibid*., 2009, vol. 43, no. 3, pp. 313−321.
23. Abiev, R.Sh, *Ibid*., 2010, vol. 44, no. 1, pp. 88−103.
24. Abiev, R.Sh., *Ibid*., 2011, vol. 45, no. 2, pp. 251−263.
25. Abiev, R.Sh. and Lavretsov, I.V., *Ibid*., 2011, vol. 45, no. 3, pp.170−177.
26. Fukano, T., Kariyasaki, A., and Ide, H., *3rd Int. Conf. on Microchannels and Minichannels*, Toronto, 2005.
27. Thulasidas, T.C., Abraham, M.A., and Cerro, R.L., *Chem. Eng. Sci*., 1995, vol. 50, no. 2, pp. 183−199.
28. Liu, H., Vandu, C. O., and Krishna, R., *Ind. Eng. Chem. Res*., 2005, vol. 44, no. 14, pp. 4884−4897.
29. Taylor, G.I., *J. Fluid Mech*., 1961, vol. 10, no. 2, pp. 161−165.
30. Bretherton, F.P., *Ibid*., 1961, vol. 10, no. 2, pp. 166−188.
31. Aussillous, P. and Quéré, D., *Phys. Fluids*, 2000, vol. 15, no. 10, pp. 2367−2371.
32. Abiev, R.Sh., Abstracts of Papers, *Mezhd. Konf. "Matematicheskie metody v tekhnike i tekhnologiyakh"* (Int. Conf. "Mathematical Methods in Technics and Technologies"), Pskov, 2009.

33. Abiev, R.Sh., Abstracts of Papers, *Mezhd. Konf. "Matematicheskie metody v tekhnike i tekhnologiyakh"* (Int. Conf. "Mathematical Methods in Technics and Technologies"), Saratov, 2008.
34. Thulasidas, T.C., Abraham, M.A., and Cerro, R.L., *Chem. Eng. Sci*., 1997, vol. 52, no. 17, pp. 2947−2962.
35. Tsoligkas, A.N., Simmons, M.J.H., and Wood, J., *6th Int. Conf. on Multiphase Flow*, Leipzig, 2007.
36. Mishima, K. and Hibiki, T., *Int. J. Multiphase Flow*, 1996, vol. 22, no. 4, pp. 703−712.
37. Laborie, S., Cabassud, C., Durand-Bourlier, L., and Laine, J.M., *Chem. Eng. Sci*., 1999, vol. 54, no. 23, pp. 5723−5735.
38. Armand, A.A. and Treshchev, G.G., *Izv. Vses. Teplotekh. Inst*., 1946, vol. 15, no. 1, pp. 16−23.
39. Kawahara, A. and Chung, P.M.-Y., *Int. J. Multiphase Flow*, 2002, vol. 28, no. 9, pp. 1411−1435.
40. Chung, P.M.-Y. and Kawaji, M., *Ibid*., 2004, vol. 30, nos. 7–8, pp. 735−761.
41. Heiszwolf, J.J., Engelvaart, L.B., van den Eijnden, M.T., et al., *Chem. Eng. Sci*., 2001, vol. 56, no. 3, pp. 805−812.
42. Serizawa, A., Feng, Z., and Kawara, Z., Exp. *Thermal Fluid Sci*., 2002, vol. 26, nos. 6–7, pp. 703−714.
43. Warnier, M.J.F., de Croon, M.H.J.M., Rebrov, E.V., and Schouten, J.C., *Microfluid. Nanofluid*., 2010, vol. 8, no. 1, pp. 33−45.
44. Chalfi, T.Y. and Ghiaasiaan, S.M., *Int. J. Multiphase Flow*, 2008, vol. 34, no. 1, pp. 2−12.
45. Lockhart, R.W. and Martinelli, R.C., *Chem. Eng. Progr*., 1949, vol. 45, no. 1, pp. 39−48.
46. Chisholm, D. and Laird, A.D.K., *Trans. ASME*, 1958, vol. 80, no. 2, pp. 276−286.
47. Chisholm, D., *Int. J. Heat Mass Transfer*, 1967, vol. 10, no. 12, pp. 1767−1778.
48. Grolman, E., Edvinsson, R., Stankiewicz, A., and Moulijn, J., *Proc. ASME Heat Transfer Div*., 1996, vol. 334, no. 3, pp. 171–178.
49. Reinecke, N. and Mewes, D., *Int. J. Multiphase Flow*, 1999, vol. 25, nos. 6−7, pp. 1373–1393.
50. Liang, S.B. and Ma, H.B., *Int. Comm. Heat Mass Transfer*, 2004, vol. 31, no. 3, pp. 365–375.
51. van Steijn, V., Kreutzer, M.T., and Kleijn, C.R., *Chem. Eng. J*., 2007, vol. 135, pp. 159−165.
52. Dessimoz, A.L., Cavin, L., Renken, A., and Kiwi-Minsker, L., *Chem. Eng. Sci*., 2008, vol. 63, no. 16, pp. 4035–4044.
53. de Tezanos Pinto, M., Abraham, M.A., and Cerro, R.L., *Ibid*., 1997, vol. 52, no.11, pp. 1685−1700.
54. van Steijn, V., Kreutzer, M.T., and Kleijn, C.R., *Ibid*., 2007, vol. 62, no. 24, pp. 7505−7514.
55. Hibiki, T. and Mishima, K., *Nucl. Eng. Design*, 2001, vol. 203, nos. 2–3, pp. 117−131.
56. Hetsroni, G., Mosyak, A., Segal, Z., and Pogrebnyak, E., *Int. J. Multiphase Flow*, 2003, vol. 29, no. 3, pp. 341–360.
57. Bauer, T., *Dissertation, Technische Universitat Dresden*, Dresden, 2007.
58. Suo, M. and Griffith, P., *J. Basic Eng.,* 1964, vol. 86, no. 3, pp. 576−582.
59. Triplett, K.A., Ghiaasiaan, S.M., Abdel-Khalik, S.I., and Sadowski, D.L., *Int. J. Multiphase Flow*, 1999, vol. 25, no. 3, pp. 377−394.
60. Dowe, D.C. and Rezkallah, K.S., *Int. J. Multiphase Flow*, 1999, vol. 25, no. 3, pp. 433−457.
61. Jayawardena, S.S., Balakotaiah, V., and Witte, L., *AIChE J*., 1997, vol. 43, no. 6, pp. 1637–1640.
62. Hatziantoniou, V. and Andersson, B., *Ind. Eng. Chem. Fundam*., 1982, vol. 21, no. 4, pp. 451−456.
63. Horvath, C., Solomon, B.A., and Engasser, J-M., *Ibid*., 1973, vol. 12, no. 4, pp. 431−439.
64. Kreutzer, M.T., Du, P., Heiszwolf, J.J., Kapteijn, F., and Moulijn, J.A., *Chem. Eng. Sci*., 2001, vol. 56, no. 22, pp. 6015−6023.
65. Heiszwolf, J.J., Kreutzer, M.T., van den Eijnden, M.G., Kapteijn, F., and Moulijn, J.A., *Catal. Today*, 2001, vol. 69, nos. 1–4, p. 51.
66. Gruber, R. and Melin, T., *Int. J. Heat Mass Transfer*, 2003, vol. 46, no. 15, pp. 2799−2808.
67. Van Baten, J.M. and Krishna, R., *Chem. Eng. Sci*., 2004, vol. 59, no. 12, pp. 2535−2545.
68. Sherwood, T. K., Pigford, R. L., and Wilke, C.R., *Mass Transfer,* New York: McGraw-Hill, 1975.
69. Vandu, C.O., Ellenberger, J., and Krishna, R., *Chem. Eng. Proc*., 2005, vol. 44, no. 3, pp. 363−374.
70. Vandu, C. O., Liu, H., and Krishna, R., *Chem. Eng. Sci*., 2005, vol. 60, no. 22, pp. 6430−6437.
71. Tsoligkas, A.N., Simmons, M.J.H., Wood, J., and Frost, C.G., *Catal. Today*, 2007, vol. 128, nos. 1−2, p. 3646.